

Noether-Constrained Correlations in Equilibrium Liquids

Florian Sammüller,¹ Sophie Hermann,¹ Daniel de las Heras,¹ and Matthias Schmidt¹

¹*Theoretische Physik II, Physikalisches Institut, Universität Bayreuth, D-95447 Bayreuth, Germany*

(Dated: 26 January 2023; revised version: 7 June 2023)

Liquid structure carries deep imprints of an inherent thermal invariance against a spatial transformation of the underlying classical many-body Hamiltonian. At first order in the transformation field Noether's theorem yields the local force balance. Three distinct two-body correlation functions emerge at second order, namely the standard two-body density, the localized force-force correlation function, and the localized force gradient. An exact Noether sum rule interrelates these correlators. Simulations of Lennard-Jones, Yukawa, soft-sphere dipolar, Stockmayer, Gay-Berne and Weeks-Chandler-Andersen liquids, of monatomic water and of a colloidal gel former demonstrate the fundamental role in the characterization of spatial structure.

It is a both surprising and intriguing phenomenon that the liquid phase occurs in the phase diagram at and off coexistence with the gas or the solid phase. Famously it has been argued [1, 2] that it needs relying on observations rather than mere theory alone to predict the existence of liquids, as neither the noninteracting ideal gas nor the Einstein crystal form appropriate idealized references. The liquid state [3–6] comprises high spatial symmetry against global translations and rotations, together with the correlated and strongly interacting behaviour of the dense constituents, whether they are atoms, molecules, or colloids.

Among the defining features of liquids are the ability to spontaneously form an interface when at liquid-gas coexistence, the viscous response against shearing motion, and the rich pair correlation structure. While the one-body density distribution is homogeneous in bulk (in stark contrast to the microscopic density of a crystal), the joint probability of finding two particles at a given separation distance r is highly nontrivial in a liquid. The pair correlation function $g(r)$ [4], as accessible e.g. via microscopy [7–10] and scattering [4, 11–14] techniques, quantifies this spatial structure on the particle level. At large distances r , the asymptotic decay of $g(r)$ falls into different classes [15–18] with much current interest in electrolytes [19]. The spatial Fourier transform of $g(r)$ is the static structure factor [4, 11–14].

It is a common strategy to exploit the symmetries of a given physical system via Noether's theorem of invariant variations [20, 21]. From symmetries in the dynamical description of the system one systematically obtains conservation laws. Typically the starting point is the action functional, as generalized to a variety of statistical mechanical settings [22–30]. In contrast, we have recently applied Noether's concept directly to statistical mechanical functionals, such as the free energy [31–34]. This allows to exploit a specific thermal invariance property of Hamiltonian many-body systems against shifting as performed globally [31–33] or locally resolved in position [34, 35].

In this Letter we demonstrate that at the local second-order level the thermal Noether invariance leads to exact

identities (“sum rules” [4, 36–43]) that form a comprehensive statistical two-body correlation framework. We use simulations to demonstrate the relevance for the investigation of the structure of simple, beyond-simple and gelled liquids.

We consider systems of N classical particles in three dimensions with positions $\mathbf{r}_1, \dots, \mathbf{r}_N \equiv \mathbf{r}^N$ and momenta $\mathbf{p}_1, \dots, \mathbf{p}_N \equiv \mathbf{p}^N$. The Hamiltonian consists of kinetic, interparticle, and external energy contributions,

$$H = \sum_i \frac{\mathbf{p}_i^2}{2m} + u(\mathbf{r}^N) + \sum_i V_{\text{ext}}(\mathbf{r}_i), \quad (1)$$

where the indices $i = 1, \dots, N$ run over all particles, m indicates the particle mass, $u(\mathbf{r}^N)$ is the interparticle interaction potential, and $V_{\text{ext}}(\mathbf{r})$ is a one-body external potential as a function of position \mathbf{r} .

We consider a canonical transformation [44], where coordinates and momenta change according to the following map [35]:

$$\mathbf{r}_i \rightarrow \mathbf{r}_i + \boldsymbol{\epsilon}(\mathbf{r}_i), \quad (2)$$

$$\mathbf{p}_i \rightarrow [\mathbb{1} + \nabla_i \boldsymbol{\epsilon}(\mathbf{r}_i)]^{-1} \cdot \mathbf{p}_i. \quad (3)$$

Here $\boldsymbol{\epsilon}(\mathbf{r})$ is a spatial “shifting” field that parameterizes the transform, $\mathbb{1}$ indicates the 3×3 -unit matrix, the superscript -1 of a matrix is its inverse, and ∇_i indicates the derivative with respect to \mathbf{r}_i , such that $\nabla_i \boldsymbol{\epsilon}(\mathbf{r}_i)$ is a 3×3 -matrix. The transformation (2) and (3) preserves both the phase space volume element and the Hamiltonian [35, 44]; its self-adjoint version is applicable to quantum systems [34]. The form of the vector field $\boldsymbol{\epsilon}(\mathbf{r})$ must be such that the transformation between original and new coordinates is bijective [34].

We consider the shifting field and its gradient to be small and hence Taylor expand. The coordinate transformation (2) is already linear in the displacement field and is hence unaffected. The momentum transformation (3), when expanded as a geometric (Neumann) series to second order, is:

$$[\mathbb{1} + \nabla_i \boldsymbol{\epsilon}(\mathbf{r}_i)]^{-1} = \mathbb{1} - \nabla_i \boldsymbol{\epsilon}(\mathbf{r}_i) + [\nabla_i \boldsymbol{\epsilon}(\mathbf{r}_i)]^2 - \dots, \quad (4)$$

where the exponents on the right hand side imply matrix products such that $[\nabla_i \epsilon(\mathbf{r}_i)]^2 = [\nabla_i \epsilon(\mathbf{r}_i)] \cdot [\nabla_i \epsilon(\mathbf{r}_i)]$, etc. When expressed in the new variables, the Hamiltonian acquires a functional dependence on the shifting field, i.e. $H \rightarrow H[\epsilon]$. It is then straightforward to show [34, 35] that the locally resolved one-body force operator $\hat{\mathbf{F}}(\mathbf{r})$ follows from functional differentiation according to:

$$-\left. \frac{\delta H[\epsilon]}{\delta \epsilon(\mathbf{r})} \right|_{\epsilon=0} = \hat{\mathbf{F}}(\mathbf{r}), \quad (5)$$

where $\delta/\delta \epsilon(\mathbf{r})$ indicates the functional derivative with respect to the shifting field $\epsilon(\mathbf{r})$. As indicated, $\epsilon(\mathbf{r})$ is set to zero after the derivative has been taken. Similar to the structure of the Hamiltonian (1), the one-body force operator $\hat{\mathbf{F}}(\mathbf{r})$ contains kinetic, interparticle, and external contributions:

$$\hat{\mathbf{F}}(\mathbf{r}) = -\nabla \cdot \sum_i \frac{\mathbf{p}_i \mathbf{p}_i}{m} \delta(\mathbf{r} - \mathbf{r}_i) + \hat{\mathbf{F}}_{\text{int}}(\mathbf{r}) - \hat{\rho}(\mathbf{r}) \nabla V_{\text{ext}}(\mathbf{r}). \quad (6)$$

Here $\delta(\cdot)$ indicates the (three-dimensional) Dirac distribution, $\hat{\mathbf{F}}_{\text{int}}(\mathbf{r}) = -\sum_i \delta(\mathbf{r} - \mathbf{r}_i) \nabla_i u(\mathbf{r}^N)$ is the interparticle one-body force operator [45], and $\hat{\rho}(\mathbf{r}) = \sum_i \delta(\mathbf{r} - \mathbf{r}_i)$ is the standard one-body density operator [4, 5]. All considerations so far are general and hold per microstate.

We complement this deterministic description by the statistical mechanics of the grand ensemble at chemical potential μ and temperature T . The grand potential is $\Omega = -k_B T \ln \Xi$, with the the grand partition sum $\Xi = \text{Tr} e^{-\beta(H - \mu N)}$. Here k_B indicates the Boltzmann constant, $\beta = 1/(k_B T)$ denotes inverse temperature, and the classical ‘‘trace’’ operation in the grand ensemble is given by $\text{Tr} \cdot = \sum_{N=0}^{\infty} (N! h^{3N})^{-1} \int d\mathbf{r}_1 \dots d\mathbf{r}_N \int d\mathbf{p}_1 \dots d\mathbf{p}_N \cdot$, where h denotes the Planck constant. The corresponding grand probability distribution is $\Psi = e^{-\beta(H - \mu N)}/\Xi$ and thermal averages are defined via $\langle \cdot \rangle = \text{Tr} \Psi \cdot$, as is standard. A primary example of a thermal average is the density profile being the average of the one-body density operator, i.e. $\rho(\mathbf{r}) = \langle \hat{\rho}(\mathbf{r}) \rangle$.

Via the transformed Hamiltonian $H[\epsilon]$, the grand partition sum acquires functional dependence on the shifting field [34, 35], i.e. $\Xi[\epsilon]$, and so does the grand potential, i.e. $\Omega[\epsilon]$. Noether invariance [31, 32] however implies that the grand potential does not change under the transformation, and hence

$$\Omega[\epsilon] = \Omega, \quad (7)$$

irrespectively of the form of $\epsilon(\mathbf{r})$. The first functional derivative of Eq. (7) with respect to the shifting field $\epsilon(\mathbf{r})$ then yields [34, 35] the locally resolved equilibrium force density balance relation $\mathbf{F}(\mathbf{r}) = \langle \hat{\mathbf{F}}(\mathbf{r}) \rangle = 0$ [4, 45].

Here we work at the second-order level and hence consider the second derivative of Eq. (7), which yields

$$\left. \frac{\delta^2 \Omega[\epsilon]}{\delta \epsilon(\mathbf{r}) \delta \epsilon(\mathbf{r}')} \right|_{\epsilon=0} = 0. \quad (8)$$

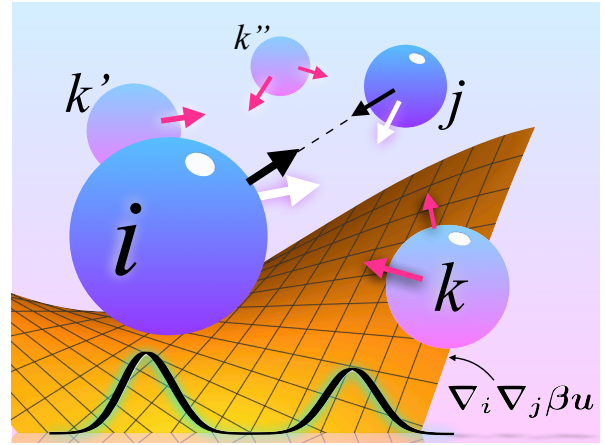


FIG. 1: Illustration of the three different correlation functions that are constrained by thermal Noether invariance. The particles (spheres) exert forces (arrows) onto each other. Particles i and j interact directly with each other (black arrows). The total force (white arrow) on each particle is also determined by the forces that all other particles k, k', k'' exert (pink arrows). The force-force correlations are balanced by the potential energy curvature $\nabla_i \nabla_j \beta u(\mathbf{r}^N)$ (orange surface) and by the two-body density Hessian $\nabla \nabla' \rho_2(\mathbf{r}, \mathbf{r}')$ (black curve).

Evaluating the functional derivative on the left hand side gives

$$\frac{\delta^2 \Omega[\epsilon]}{\delta \epsilon(\mathbf{r}) \delta \epsilon(\mathbf{r}')} = -\beta \text{cov} \left(\frac{\delta H[\epsilon]}{\delta \epsilon(\mathbf{r})}, \frac{\delta H[\epsilon]}{\delta \epsilon(\mathbf{r}')} \right) + \left\langle \frac{\delta^2 H[\epsilon]}{\delta \epsilon(\mathbf{r}) \delta \epsilon(\mathbf{r}')} \right\rangle, \quad (9)$$

where the covariance of two observables (phase space functions) \hat{A} and \hat{B} is defined in the standard way as $\text{cov}(\hat{A}, \hat{B}) = \langle \hat{A} \hat{B} \rangle - \langle \hat{A} \rangle \langle \hat{B} \rangle$. Rewriting the derivative $\delta H[\epsilon]/\delta \epsilon(\mathbf{r})$ as the negative force density operator via Eq. (5), inserting Eq. (9) into Eq. (8), and re-arranging gives the following locally resolved two-body Noether sum rule:

$$\beta \langle \hat{\mathbf{F}}(\mathbf{r}) \hat{\mathbf{F}}(\mathbf{r}') \rangle = \left\langle \frac{\delta^2 H[\epsilon]}{\delta \epsilon(\mathbf{r}) \delta \epsilon(\mathbf{r}')} \right\rangle \Big|_{\epsilon=0}. \quad (10)$$

We have replaced $\text{cov}(\hat{\mathbf{F}}(\mathbf{r}), \hat{\mathbf{F}}(\mathbf{r}')) = \langle \hat{\mathbf{F}}(\mathbf{r}) \hat{\mathbf{F}}(\mathbf{r}') \rangle$, because $\langle \hat{\mathbf{F}}(\mathbf{r}) \rangle = 0$ in equilibrium [4, 45]. The sum rule (10) relates the force-force correlations at two different positions (left hand side) with the mean curvature of the Hamiltonian with respect to variation in the shifting field (right hand side). That such physically meaningful averages are related to each other, at all positions \mathbf{r} and \mathbf{r}' , is highly nontrivial.

We can bring the fundamental Noether two-body sum rule (10) into a more convenient form by multiplying by β , splitting off the trivial kinetic contributions, and introducing the potential energy force operator $\hat{\mathbf{F}}_U(\mathbf{r})$, which combines interparticle and external forces according to $\hat{\mathbf{F}}_U(\mathbf{r}) = \hat{\mathbf{F}}_{\text{int}}(\mathbf{r}) - \hat{\rho}(\mathbf{r}) \nabla V_{\text{ext}}(\mathbf{r})$. Fur-

thermore we focus on the distinct contributions (subscript “dist”) such that only pairs of particles with unequal indices are involved and double sums reduce to $\sum_{ij(\neq)} \equiv \sum_{i=1}^N \sum_{j=1, j \neq i}^N$. This allows to identify from Eq. (10) the following exact distinct two-body Noether identity:

$$\left\langle \beta \hat{\mathbf{F}}_U(\mathbf{r}) \beta \hat{\mathbf{F}}_U(\mathbf{r}') \right\rangle_{\text{dist}} = \nabla \nabla' \rho_2(\mathbf{r}, \mathbf{r}') \quad (11)$$

$$+ \left\langle \sum_{ij(\neq)} \delta(\mathbf{r} - \mathbf{r}_i) \delta(\mathbf{r}' - \mathbf{r}_j) \nabla_i \nabla_j \beta u(\mathbf{r}^N) \right\rangle.$$

Here the two-body density is defined as is standard: $\rho_2(\mathbf{r}, \mathbf{r}') = \langle \hat{\rho}(\mathbf{r}) \hat{\rho}(\mathbf{r}') \rangle_{\text{dist}} = \langle \sum_{ij(\neq)} \delta(\mathbf{r} - \mathbf{r}_i) \delta(\mathbf{r}' - \mathbf{r}_j) \rangle$. The relationship between the different correlators, as graphically illustrated in Fig. 1, holds in general inhomogeneous situations with no need for specific simplifying symmetries.

We demonstrate that this framework has profound implications already for a bulk liquid, where $\rho(\mathbf{r}) = \rho_b = \text{const}$ and $V_{\text{ext}}(\mathbf{r}) = 0$, such that $\hat{\mathbf{F}}_U(\mathbf{r}) = \hat{\mathbf{F}}_{\text{int}}(\mathbf{r})$. In view of the form of the distinct sum rule (11), we use the pair correlation function $g(|\mathbf{r} - \mathbf{r}'|) = \rho_2(\mathbf{r}, \mathbf{r}') / \rho_b^2$, and introduce both the force-force pair correlation function $\mathbf{g}_{ff}(|\mathbf{r} - \mathbf{r}'|) = \beta^2 \langle \hat{\mathbf{F}}_{\text{int}}(\mathbf{r}) \hat{\mathbf{F}}_{\text{int}}(\mathbf{r}') \rangle_{\text{dist}} / \rho_b^2$, and the force gradient correlator $\mathbf{g}_{\nabla f}(|\mathbf{r} - \mathbf{r}'|) = -\langle \sum_{ij(\neq)} \delta(\mathbf{r} - \mathbf{r}_i) \delta(\mathbf{r}' - \mathbf{r}_j) \nabla_i \nabla_j \beta u(\mathbf{r}^N) \rangle / \rho_b^2$, which is also the negative mean potential curvature. The identity (11) can then be written succinctly as:

$$\nabla \nabla g(r) + \mathbf{g}_{\nabla f}(r) + \mathbf{g}_{ff}(r) = 0, \quad (12)$$

where $r = |\mathbf{r} - \mathbf{r}'|$ denotes the separation distance between the two positions. Both $\mathbf{g}_{ff}(r)$ and $\mathbf{g}_{\nabla f}(r)$ have tensor rank two, i.e. they are 3×3 -matrices. Given the central role that $g(r)$ plays in the theory of liquids [4], Eq. (12) is highly remarkable as it allows to express $g(r)$ via spatial integration of two seemingly entirely different (force-gradient and force-force) correlators. Due to the rotational symmetry of the bulk liquid, the only nontrivial tensor components are parallel (\parallel) and transversal (\perp) to $\mathbf{r} - \mathbf{r}'$, such that Eq. (12) reduces to

$$g''(r) + g_{\nabla f \parallel}(r) + g_{ff \parallel}(r) = 0, \quad (13)$$

$$g'(r)/r + g_{\nabla f \perp}(r) + g_{ff \perp}(r) = 0, \quad (14)$$

with the prime(s) denoting the derivative(s) with respect to r . In the chosen coordinate system the matrices are diagonal, $\text{diag}(\parallel, \perp, \perp)$, with the first axis being parallel to $\mathbf{r} - \mathbf{r}'$. For molecular liquids of particles with orientational degrees of freedom [4, 46–48] our theory, including Eqs. (13) and (14), remains valid upon equilibrium orientational averaging.

For simple fluids, where the particles interact mutually only via a pair potential $\phi(r)$, the force gradient correlator reduces to $\mathbf{g}_{\nabla f}(r) = \beta g(r) \nabla \nabla \phi(r)$ such that

$$g_{\nabla f \parallel}(r) = \beta g(r) \phi''(r), \quad g_{\nabla f \perp}(r) = \beta g(r) \phi'(r)/r. \quad (15)$$

This simplification is due to the reduction of the mixed derivative $\nabla_i \nabla_j u(\mathbf{r}^N) = \nabla_i \nabla_j \sum_{kl(\neq)} \phi(|\mathbf{r}_k - \mathbf{r}_l|)/2 = \nabla_i \nabla_j \phi(|\mathbf{r}_i - \mathbf{r}_j|)$, for $i \neq j$. This allows to rewrite the curvature correlator in Eqs. (13) and (14), which attain the form $g''(r) + \beta \phi''(r) g(r) + g_{ff \parallel}(r) = 0$ and $g'(r)/r + \beta \phi'(r) g(r)/r + g_{ff \perp}(r) = 0$. In the gas phase the validity can be analytically verified on the second virial level, where $g(r) = \exp(-\beta \phi(r))$ and the force-force correlations are due to the antiparallel direct forces between a particle pair: $g_{ff \parallel}(r) = -g(r) [\beta \phi'(r)]^2$. Furthermore $g_{ff \perp}(r) = 0$ due to the absence of a third particle at $\rho_b \rightarrow 0$ that could mediate a transversal force.

We substantiate this Noether correlation framework with computer simulations using adaptive Brownian dynamics [49], which is an algorithm that is both fast and allows for tight control of force evaluation errors. We first investigate the Lennard-Jones (LJ) liquid, the purely repulsive Weeks-Chandler-Andersen (WCA) liquid, monatomic water [50, 51], and a three-body colloidal gel former [52, 53]. The results are summarized in Fig. 2; the top line gives the respective values of T and $\rho_b = N/V$ with box volume $V = (10\sigma)^3$; the LJ potential is truncated at $r/\sigma = 2.5$ with σ denoting the respective particle size. We first discuss the two simple liquids. Both the LJ and the WCA liquid feature pair correlation functions $g(r)$ that display the familiar strongly structured, damped oscillatory form [4, 15, 16], with a prominent first peak indicating a nearest neighbor correlation shell and subsequent, increasingly washed out oscillations at larger distances. In stark contrast, both the force-gradient (potential curvature) correlator $\mathbf{g}_{\nabla f}(r)$ and the force-force correlator $\mathbf{g}_{ff}(r)$ have very different forms than $g(r)$ itself. The curvature correlator has very strongly localized positive (\parallel) and negative (\perp) peaks near $r = \sigma$. This feature is due to the strong first peak of $g(r)$ combined with the properties of $\phi'(r)$ and $\phi''(r)$, as is evident via Eq. (15), which we find to be satisfied to high numerical accuracy. Our results confirm the expectation [16] that $g(r)$ is hardly affected by interparticle attraction. In contrast the force gradient $g_{\nabla f \perp}(r)$ has a clear and significant peak in the attractive region of the LJ potential with no such feature occurring in the purely repulsive WCA liquid.

The force-force correlator $\mathbf{g}_{ff}(r)$ has a similar first peak structure as the curvature correlator, but oscillations extend much further out to larger distances r . Hence $\mathbf{g}_{ff}(r)$ captures also the indirect interactions that are mediated by surrounding particles; we recall Fig. 1. The strong negative double peak of the parallel component indicates anti-correlated force orientations, which reflect the direct interactions between pairs of particles. Both tensor components of $\mathbf{g}_{ff}(r)$ satisfy the Noether sum rules (13) and (14) to excellent numerical accuracy.

To go beyond simple liquids, we first turn to the monatomic water model by Molinero and Moore [50], which includes three-body interparticle interactions in

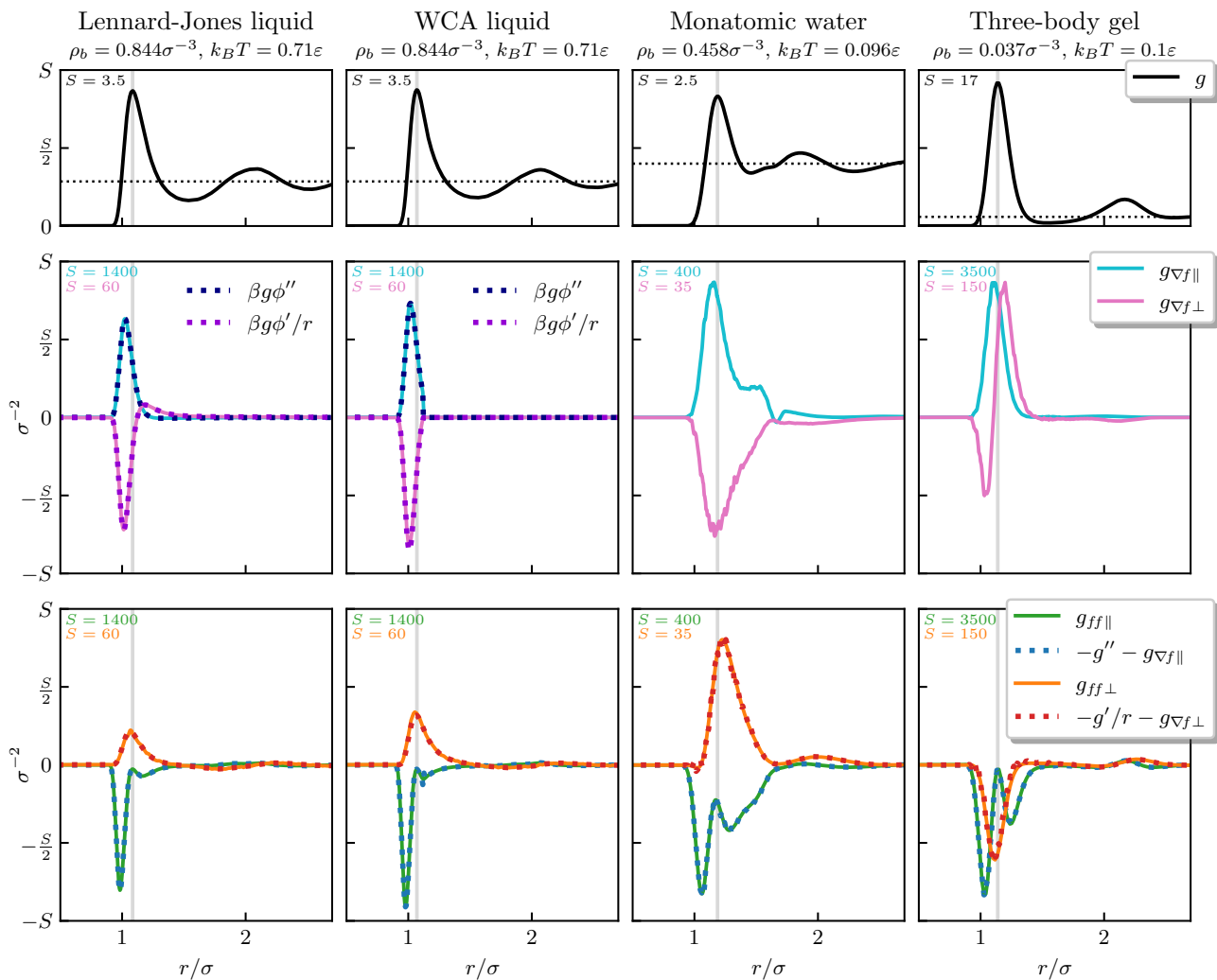


FIG. 2: Simulation results for the two-body correlation functions of the Lennard-Jones liquid (first column), the WCA liquid (second column), monatomic water (third column), and the three-body gel (fourth column). Results are shown as a function of the scaled interparticle distance r/σ , S is a vertical scale factor given in the upper left corner of each panel, and ϵ denotes the energy scale of the respective model fluid. Shown is the pair correlation function $g(r)$ (top row), the potential curvature correlator $\mathbf{g}_{\nabla f}(r)$ (middle row) and the force-force correlator $\mathbf{g}_{ff}(r)$ (bottom row); the latter two correlators have a transversal (\perp) and a parallel (\parallel) tensor component. The results for $\mathbf{g}_{\nabla f}(r)$ for the LJ and WCA liquids are numerically identical to those from the analytical expressions (15) (dashed lines). The directly sampled results for $\mathbf{g}_{ff}(r)$ are numerically identical to those obtained from the Noether sum rules (13) and (14) (dashed lines) for all four systems. Vertical gray lines indicate the position of the first maximum of $g(r)$ as a guide to the eye.

$u(\mathbf{r}^N)$ that generate the tetrahedral coordination of liquid water. The monatomic water model gives a surprisingly accurate description of the properties of real water, see Ref. [51] for very recent work, while the particles remain spherical and there is no necessity to explicitly invoke molecular orientational degrees of freedom. Hence our framework (13) and (14) applies. The third column of Fig. 2 demonstrates at ambient conditions that while the shape of $g(r)$ is similar to that in the LJ liquid, both the potential energy curvature and the force-force correlator differ markedly from those of the LJ model. Notably the shape of the double negative peak of $g_{ff\parallel}(r)$ differs and

the sign of $g_{ff\perp}(r)$ does not turn negative for distances towards the second shell, as is the case in the LJ liquid. Consistently, the magnitude of the \parallel component is much larger than the \perp component, as direct interparticle interactions are prominent in the former, whereas mediation by third particles is required for the latter.

The three-body gel former by Kob and coworkers [52, 53] alters the preferred angle of the three-body interaction term from tetrahedral to stretched (we use 180 degrees [54]). This change induces an affinity for the formation of chains while retaining an ability for their branching and thus the model forms networks in equilibrium. The

results shown in the fourth column of Fig. 2 indicate markedly different behaviour as compared to the above liquids. While $g(r)$ has the generic long-range decay that one expects of network-forming systems, both the curvature and the force-force correlator are much more specific indicators. In particular we attribute the striking shape of the transversal (\perp) tensor component to the network connectivity. Again the sum rules are satisfied to very good numerical accuracy which we take i) as a demonstration that the gel state is indeed equilibrated, which distinguishes this model [52, 53] from genuine nonequilibrium gel formers, and ii) as a confirmation of the fitness of the Noether correlators to systematically quantify complex spatial structure formation. This holds beyond the presented model fluids; see the Supplementary Information [55] for results for screened long-ranged interparticle forces of Yukawa type, as well as for dipolar [56–60], Stockmayer [60], and (isotropic and nematic) Gay-Berne fluids [60–62]. For the LJ model, we also contrast the behaviour in the liquid against both the gas and the crystal, where the identities (13) and (14) remain valid [55]. Our equilibrium theory requires proper thermal averaging for the presented identities to hold. A trivial counterexample is a precipitous temperature quench where the distribution of microstates remains instantaneously intact, but β has acquired a new value. Then the sum rule (12) is immediately violated, due to the respective scaling of the correlators $\nabla\nabla g(r)$, $\mathbf{g}_{\nabla f}(r)$, and $\mathbf{g}_{ff}(r)$ with powers β^0 , β^1 , and β^2 .

In conclusion, we have formulated and tested a systematic two-body correlation framework based on invariance against an intrinsic symmetry of thermal many-body systems. Formal similarities exist with sum rules for interfacial Hamiltonians [63], as used for studies of wetting [64], and with Takahashi-Ward identities [65, 66] of quantum field theory. Future work could relate to the effective temperature [67], to one-dimensional systems [68–70], the structure of crystals [71–73], gels [52, 53, 74], glasses [75–77] and the hexatic phase [78], to force-sampling simulation techniques [79–81], and to force-based classical [35, 82] and quantum density functional theory [83, 84]. Testing sum rules in charged systems is valuable, but can be technically subtle [85]. Connections to three-point [77] and four-point [86, 87] correlation functions are interesting, as for a simple fluid $\mathbf{g}_{ff}(r)$ is given via two position integrals over the four-body density. We have checked that for molecular liquids the general force correlation sum rules (10) and (11) remain valid upon supplementing the dependence on positions \mathbf{r}, \mathbf{r}' with dependence on the molecular orientational degrees of freedom; an analogous structure holds for mixtures of different components. Deriving torque correlation sum rules requires using a local version of the Noether rotational invariance [31].

A particularly exciting prospect is to apply the general identity (11) to the study of interfacial phenomena [38–41, 43, 51], where the connections with the existing

body of sum rules [4, 36–43] and the constraints that follow on the allowed correlation function structure at complete drying [88–90] and wetting transitions are worth exploring. Besides measurements of $g(r)$ [7–13], position-resolved forces have recently become accessible by direct imaging in colloidal systems [91], which can facilitate experimental investigations of Noether correlators.

We thank Andrew O. Parry for pointing out Ref. [63] to us, and we are grateful to him, Gerhard Jung, Atreyee Banerjee, Liesbeth Janssen, and Marjolein Dijkstra for useful discussions.

-
- [1] V. F. Weisskopf, About Liquids, Trans. N. Y. Acad. Sci. **38**, 202 (1977).
 - [2] R. Evans, D. Frenkel, and M. Dijkstra, From simple liquids to colloids and soft matter, Phys. Today **72**, 38 (2019).
 - [3] J. A. Barker and D. Henderson, What is “liquid”? Understanding the states of matter, Rev. Mod. Phys. **48**, 587 (1976).
 - [4] J. P. Hansen and I. R. McDonald, *Theory of Simple Liquids*, 4th ed. (Academic Press, London, 2013).
 - [5] R. Evans, The nature of the liquid-vapour interface and other topics in the statistical mechanics of non-uniform, classical fluids, Adv. Phys. **28**, 143 (1979).
 - [6] R. Evans, M. Oettel, R. Roth, and G. Kahl, New developments in classical density functional theory, J. Phys.: Condens. Matter **28**, 240401 (2016).
 - [7] C. P. Royall, A. A. Louis, and H. Tanaka, Measuring colloidal interactions with confocal microscopy, J. Chem. Phys. **127**, 044507 (2007).
 - [8] A. L. Thorneywork, R. Roth, D. G. A. L. Aarts, and R. P. A. Dullens, Communication: Radial distribution functions in a two-dimensional binary colloidal hard sphere system, J. Chem. Phys. **140**, 161106 (2014).
 - [9] A. Statt, R. Pinchaipat, F. Turci, R. Evans, and C. P. Royall, Direct observation in 3d of structural crossover in binary hard sphere mixtures, J. Chem. Phys. **144**, 144506 (2016)
 - [10] A. Ramirez-Saito, C. Bechinger, and J. L. Arauz-Lara, Optical microscopy measurement of pair correlation functions, Phys. Rev. E **74**, 030401(R) (2006).
 - [11] J. L. Yarnell, M. J. Katz, R. G. Wenzel, and S. H. Koenig, Structure factor and radial distribution function for liquid argon at 85K, Phys. Rev. A **7**, 2130 (1973).
 - [12] P. S. Salmon, Decay of the pair correlations and small-angle scattering for binary liquids and glasses, J. Phys.: Condens. Matter **18**, 11443 (2006).
 - [13] F. S. Carvalho, J. P. Braga, Partial radial distribution functions for a two-component glassy solid, GeSe, from scattering experimental data using an artificial intelligence framework, J. Molec. Modeling **28**, 99 (2022).
 - [14] J. C. Dyre, Simple liquids’ quasiuniversality and the hard-sphere paradigm, J. Phys.: Condens. Matter **28**, 323001 (2016).
 - [15] R. Evans, J. R. Henderson, D. C. Hoyle, A. O. Parry, and Z. A. Sabeur, Asymptotic decay of liquid structure: oscillatory liquid-vapour density profiles and the Fisher-Widom line, Mol. Phys. **80**, 755 (1993).

- [16] R. Evans, R. J. F. Leote de Carvalho, J. R. Henderson, and D. C. Hoyle, Asymptotic decay of correlations in liquids and their mixtures, *J. Chem. Phys.* **100**, 591 (1994).
- [17] M. Dijkstra and R. Evans, A simulation study of the decay of the pair correlation function in simple fluids, *J. Chem. Phys.* **112**, 1449 (2000).
- [18] C. Grodon, M. Dijkstra, R. Evans, and R. Roth, Decay of correlation functions in hard-sphere mixtures: Structural crossover, *J. Chem. Phys.* **121**, 7869 (2004).
- [19] P. Cats, R. Evans, A. Härtel, and R. van Roij, Primitive model electrolytes in the near and far field: Decay lengths from DFT and simulations, *J. Chem. Phys.* **154**, 124504 (2021).
- [20] E. Noether, Invariante Variationsprobleme, *Nachr. d. König. Gesellsch. d. Wiss. zu Göttingen, Math.-Phys. Klasse*, **235**, 183 (1918). English translation by M. A. Tavel: Invariant variation problems. *Transp. Theo. Stat. Phys.* **1**, 186 (1971); for a version in modern typesetting see: Frank Y. Wang, arXiv:physics/0503066v3 (2018).
- [21] N. Byers, E. Noether's discovery of the deep connection between symmetries and conservation laws, arXiv:physics/9807044 (1998).
- [22] A. G. Lezcano and A. C. M. de Oca, A stochastic version of the Noether theorem, *Found. Phys.* **48**, 726 (2018).
- [23] J. C. Baez and B. Fong, A Noether theorem for Markov processes, *J. Math. Phys.* **54**, 013301 (2013).
- [24] I. Marvian and R. W. Spekkens, Extending Noether's theorem by quantifying the asymmetry of quantum states, *Nat. Commun.* **5**, 3821 (2014).
- [25] S. Sasa and Y. Yokokura, Thermodynamic entropy as a Noether invariant, *Phys. Rev. Lett.* **116**, 140601 (2016).
- [26] S. Sasa, S. Sugiura, and Y. Yokokura, Thermodynamical path integral and emergent symmetry, *Phys. Rev. E* **99**, 022109 (2019).
- [27] Y. Minami and S. Sasa, Thermodynamic entropy as a Noether invariant in a Langevin equation, *J. Stat. Mech.* **2020**, 013213 (2020).
- [28] M. Revzen, Functional integrals in statistical physics, *Am. J. Phys.* **38**, 611 (1970).
- [29] Y. A. Budkov and A. L. Kolesnikov, Modified Poisson-Boltzmann equations and macroscopic forces in inhomogeneous ionic fluids, *J. Stat. Mech.* **2022**, 053205 (2022).
- [30] P. E. Brandyshev, Y. A. Budkov, Noether's second theorem and covariant field theory of mechanical stresses in inhomogeneous ionic fluids, *J. Chem. Phys.* **158**, 174114 (2023).
- [31] S. Hermann and M. Schmidt, Noether's theorem in statistical mechanics, *Commun. Phys.* **4**, 176 (2021).
- [32] S. Hermann and M. Schmidt, Why Noether's theorem applies to statistical mechanics, *J. Phys.: Condens. Matter* **34**, 213001 (2022) (Topical Review).
- [33] S. Hermann and M. Schmidt, Variance of fluctuations from Noether invariance, *Commun. Phys.* **5**, 276 (2022).
- [34] S. Hermann and M. Schmidt, Force balance in thermal quantum many-body systems from Noether's theorem, *J. Phys. A: Math. Theor.* **55**, 464003 (2022).
- [35] S. M. Tschopp, F. Sammüller, S. Hermann, M. Schmidt, and J. M. Brader, Force density functional theory in- and out-of-equilibrium, *Phys. Rev. E* **106**, 014115 (2022).
- [36] J. R. Henderson, "Statistical mechanical sum rules," in *Fundamentals of Inhomogeneous Fluids*, edited by D. Henderson (Dekker, New York, 1992).
- [37] R. Evans, "Density functionals in the theory of non-uniform fluids," in *Fundamentals of Inhomogeneous Fluids*, edited by D. Henderson (Dekker, New York, 1992).
- [38] P. J. Upton, Fluids against hard walls and surface critical behavior, *Phys. Rev. Lett.* **81**, 2300 (1998).
- [39] R. Evans and A. O. Parry, Liquids at interfaces: what can a theorist contribute? *J. Phys.: Condens. Matter* **2**, SA15 (1990).
- [40] J. R. Henderson and F. van Swol, On the interface between a fluid and a planar wall: theory and simulations of a hard sphere fluid at a hard wall, *Mol. Phys.* **51**, 991 (1984).
- [41] J. R. Henderson and F. van Swol, On the approach to complete wetting by gas at a liquid-wall interface, *Mol. Phys.* **56**, 1313 (1985).
- [42] J. O. Hirschfelder, Classical and quantum mechanical hypervirial theorems, *J. Chem. Phys.* **33**, 1462 (1960).
- [43] D. G. Triezenberg and R. Zwanzig, Fluctuation theory of surface tension, *Phys. Rev. Lett.* **28**, 1183 (1972).
- [44] H. Goldstein, C. Poole, and J. Safko, *Classical Mechanics* (Addison-Wesley, New York, 2002). Our generator \mathcal{G} is given as F_2 in their notation.
- [45] M. Schmidt, Power functional theory for many-body dynamics, *Rev. Mod. Phys.* **94**, 015007 (2022).
- [46] S. Zhao, R. Ramirez, R. Vuilleumier, D. Borgis, Molecular density functional theory of solvation: From polar solvents to water, *J. Chem. Phys.* **134**, 194102 (2011).
- [47] G. Jeanmairet, M. Levesque, R. Vuilleumier, and D. Borgis, Molecular density functional theory of water, *J. Phys. Chem. Lett.* **4**, 619 (2013).
- [48] S. Luukkonen, M. Levesque, L. Belloni, and D. Borgis, Hydration free energies and solvation structures with molecular density functional theory in the hypernetted chain approximation, *J. Chem. Phys.* **152**, 064110 (2020).
- [49] F. Sammüller and M. Schmidt, Adaptive Brownian dynamics, *J. Chem. Phys.* **155**, 134107 (2021).
- [50] V. Molinero and E. B. Moore, Water modeled as an intermediate element between carbon and silicon, *J. Phys. Chem. B* **113**, 4008 (2009).
- [51] M. K. Coe, R. Evans, and N. B. Wilding, The coexistence curve and surface tension of a monatomic water model, *J. Chem. Phys.* **156**, 154505 (2022).
- [52] S. Saw, N. L. Ellegaard, W. Kob, and S. Sastry, Structural relaxation of a gel modeled by three body interactions, *Phys. Rev. Lett.* **103**, 248305 (2009).
- [53] S. Saw, N. L. Ellegaard, W. Kob, and S. Sastry, Computer simulation study of the phase behavior and structural relaxation in a gel-former modeled by three-body interactions, *J. Chem. Phys.* **134**, 164506 (2011).
- [54] F. Sammüller, D. de las Heras, and M. Schmidt, Inhomogeneous steady shear dynamics of a three-body colloidal gel former, *J. Chem. Phys.* **158**, 054908 (2023).
- [55] See Supplementary Information for simulation results of the Noether correlation functions for the Yukawa, soft-sphere dipolar, Stockmayer, and Gay-Berne models (Fig. 3), as well as results for the gas, liquid, and crystal phase of the Lennard-Jones model (Fig. 4).
- [56] P. I. C. Teixeira, J. M. Tavares, and M. M. Telo da Gama, Review Article: The effect of dipolar forces on the structure and thermodynamics of classical fluids, *J. Phys.: Condens. Matter* **12**, R411 (2000).
- [57] S. H. L. Klapp, Topical Review: Dipolar fluids under external perturbations, *J. Phys.: Condens. Matter* **17**, R525 (2005).
- [58] M. J. Stevens and G. S. Grest, Structure of soft-sphere

- dipolar fluids, *Phys. Rev. E* **51**, 5962 (1995).
- [59] J. M. Tavares, J. J. Weis, and M. M. Telo da Gama, Strongly dipolar fluids at low densities compared to living polymers, *Phys. Rev. E* **59**, 4388 (1999).
- [60] M. P. Allen, Topical Review: Molecular simulation of liquid crystals *Mol. Phys.* **117**, 2391 (2019).
- [61] J. G. Gay and B. J. Berne, Modification of the overlap potential to mimic a linear site-site potential *J. Chem. Phys.* **74**, 3316 (1981).
- [62] J. T. Brown, M. P. Allen, E. Martín del Río, and E. de Miguel, Effects of elongation on the phase behavior of the Gay-Berne fluid, *Phys. Rev. E* **57**, 6685 (1998).
- [63] L. V. Mikhheev and J. D. Weeks, Sum rules for interface Hamiltonians, *Physica A* **177**, 495 (1991).
- [64] A. Squarcini, J. M. Romero-Enrique, and A. O. Parry, Casimir Contribution to the Interfacial Hamiltonian for 3D Wetting, *Phys. Rev. Lett.* **128**, 195701 (2022).
- [65] J. C. Ward, An identity in quantum electrodynamics, *Phys. Rev.* **78**, 182 (1950).
- [66] Y. Takahashi, On the generalized Ward identity, *Il Nuovo Cimento* **6**, 371 (1957).
- [67] S. Saw, L. Costigliola, and J. C. Dyre, Configurational temperature in active-matter models. I. Lines of invariant physics in the phase diagram of the Ornstein-Uhlenbeck model, *Phys. Rev. E* **107**, 024609 (2023).
- [68] C. W. J. Beenakker, Pair correlation function of the one-dimensional Riesz gas, *Phys. Rev. Research* **5**, 013152 (2023).
- [69] A. Flack, S. N. Majumdar, and G. Schehr, An exact formula for the variance of linear statistics in the one-dimensional jellium model, *J. Phys. A: Math. Theor.* **56**, 105002 (2023).
- [70] A. M. Montero and A. Santos, Triangle-well and ramp interactions in one-dimensional fluids: a fully analytic exact solution, *J. Stat. Phys.* **175**, 269 (2019).
- [71] C. Walz and M. Fuchs, Displacement field and elastic constants in nonideal crystals, *Phys. Rev. B* **81**, 134110 (2010).
- [72] J. M. Häring, C. Walz, G. Szamel, and M. Fuchs, Coarse-grained density and compressibility of nonideal crystals: General theory and an application to cluster crystals, *Phys. Rev. B* **92**, 184103 (2015).
- [73] S.-C. Lin, M. Oettel, J. M. Häring, R. Haussmann, M. Fuchs, and G. Kahl, Direct correlation function of a crystalline solid, *Phys. Rev. Lett.* **127**, 085501 (2021).
- [74] B. A. Lindquist, R. B. Jadrich, D. J. Milliron, and T. M. Truskett, On the formation of equilibrium gels via a macroscopic bond limitation, *J. Chem. Phys.* **145**, 074906 (2016).
- [75] M. K. Nandi, A. Banerjee, C. Dasgupta, S. M. Bhattacharyya, Role of the pair correlation function in the dynamical transition predicted by mode coupling theory, *Phys. Rev. Lett.* **119**, 265502 (2017).
- [76] L. M. C. Janssen, Mode-coupling theory of the glass transition: A primer, *Front. Phys.* **6**, 97 (2018).
- [77] C. Luo, J. F. Robinson, I. Pihlajamaa, V. E. Debets, C. P. Royall, and L. M. C. Janssen, Many-body correlations are non-negligible in both fragile and strong glassformers, *Phys. Rev. Lett.* **129**, 145501 (2022).
- [78] E. P. Bernard and W. Krauth, Two-Step melting in two dimensions: first-order liquid-hexatic transition, *Phys. Rev. Lett.* **107**, 155704 (2011).
- [79] B. Rotenberg, Use the force! Reduced variance estimators for densities, radial distribution functions, and local mobilities in molecular simulations, *J. Chem. Phys.* **153**, 150902 (2020).
- [80] D. de las Heras and M. Schmidt, Better than counting: Density profiles from force sampling, *Phys. Rev. Lett.* **120**, 218001 (2018).
- [81] D. Borgis, R. Assaraf, B. Rotenberg, and R. Vuilleumier, Computation of pair distribution functions and three-dimensional densities with a reduced variance principle, *Mol. Phys.* **111**, 3486 (2013).
- [82] F. Sammüller, S. Hermann, and M. Schmidt, Comparative study of force-based classical density functional theory, *Phys. Rev. E* **107**, 034109 (2023).
- [83] C. A. Ullrich and I. V. Tokatly, Nonadiabatic electron dynamics in time-dependent density-functional theory, *Phys. Rev. B* **73**, 235102 (2006).
- [84] M. M. Tchenkoue, M. Penz, I. Theophilou, M. Ruggenthaler, and A. Rubio, Force balance approach for advanced approximations in density functional theories, *J. Chem. Phys.* **151**, 154107 (2019).
- [85] J. M. Falcón-González, C. Contreras-Aburto, M. Lara-Peña, M. Heinen, C. Avendaño, A. Gil-Villegas, and R. Castañeda-Priego, Assessment of the Wolf method using the Stillinger-Lovett sum rules: from strong electrolytes to weakly charged colloidal dispersions, *J. Chem. Phys.* **153**, 234901 (2020).
- [86] Z. Zhang and W. Kob, Revealing the three-dimensional structure of liquids using four-point correlation functions, *PNAS* **117**, 14032 (2020).
- [87] N. Singh, Z. Zhang, A. K. Sood, W. Kob, and R. Ganapathy, Intermediate-range order governs dynamics in dense colloidal liquids, *Proc. Nat. Acad. Sci.* **120**, e2300923120 (2023).
- [88] R. Evans, M. C. Stewart, and N. B. Wilding, A unified description of hydrophilic and superhydrophobic surfaces in terms of the wetting and drying transitions of liquids, *Proc. Nat. Acad. Sci.* **116**, 23901 (2019).
- [89] M. K. Coe, R. Evans, and N. B. Wilding, Density depletion and enhanced fluctuations in water near hydrophobic solutes: identifying the underlying physics, *Phys. Rev. Lett.* **128**, 045501 (2022).
- [90] M. K. Coe, R. Evans, and N. B. Wilding, Understanding the physics of hydrophobic solvation, *J. Chem. Phys.* **158**, 034508 (2023).
- [91] J. Dong, F. Turci, R. L. Jack, M. A. Faers, and C. P. Royall, Direct imaging of contacts and forces in colloidal gels, *J. Chem. Phys.* **156**, 214907 (2022).

Supplementary Information

Noether-Constrained Correlations in Equilibrium Liquids

Florian Sammüller, Sophie Hermann, Daniel de las Heras, and Matthias Schmidt

Theoretische Physik II, Physikalisches Institut, Universität Bayreuth, D-95447 Bayreuth, Germany

(Dated: 7 June 2023, www.mschmidt.uni-bayreuth.de)

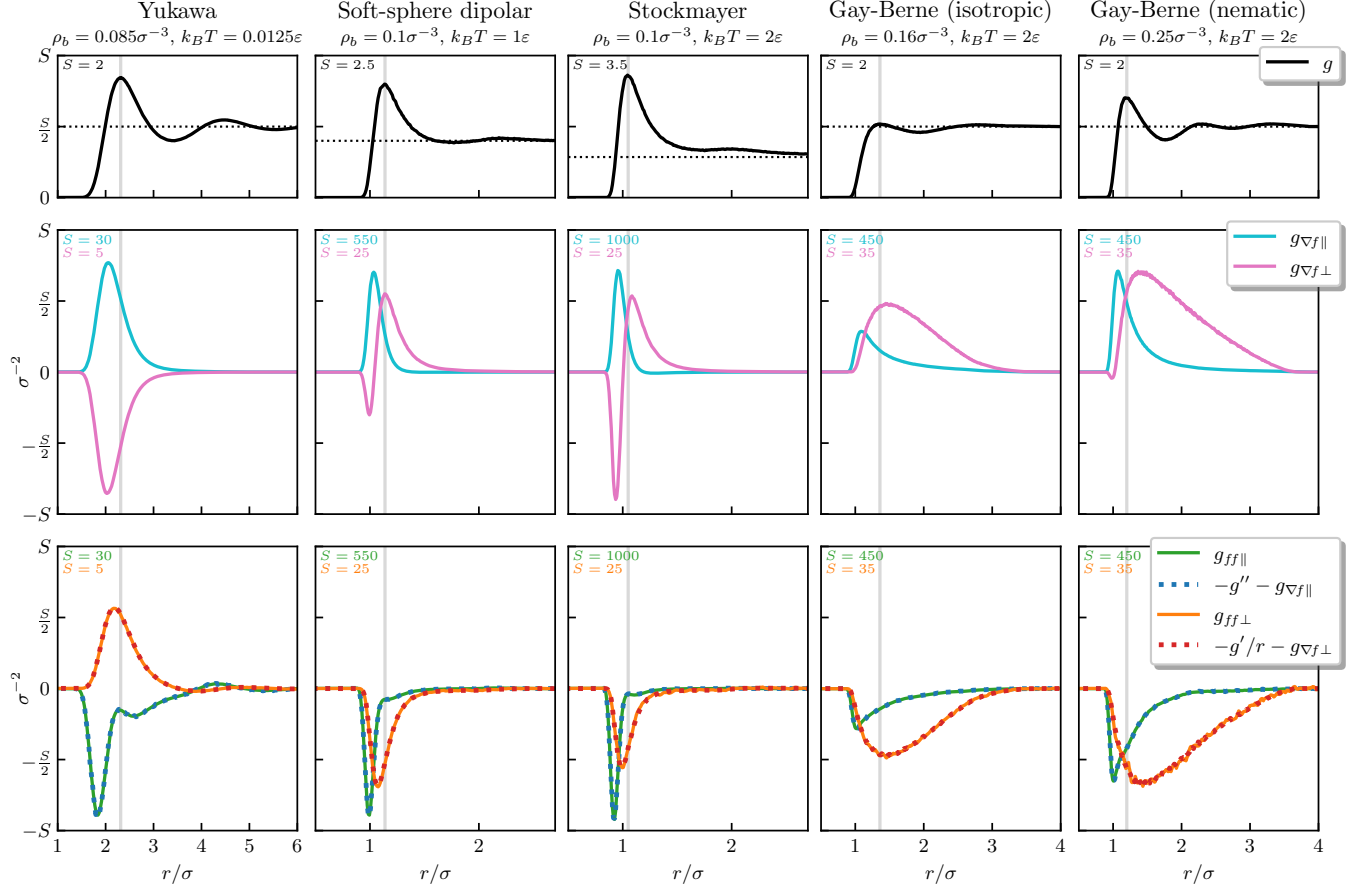


FIG. 3: Correlation functions analogous to Fig. 2 of the main text, but for the Yukawa liquid (first column), the soft-sphere dipolar fluid (second column), the Stockmayer fluid (third column), and the Gay-Berne model in the isotropic (fourth column) and nematic phase (fifth column). The results for the anisotropic models are obtained from canonical Monte Carlo simulations, and they are averaged over the microscopic orientations; the simulation box volume is $V = (20\sigma)^3$ and the long-ranged interactions are cut off at radial distance 10σ . Shown are results for the pair correlation function $g(r)$ (first row) and for the radial (\parallel) and transversal (\perp) components of the two-body force-gradient correlator $\mathbf{g}_{\nabla f}(r)$ (second row) and the force-force pair correlator $\mathbf{g}_{ff}(r)$ (third row). The respective vertical scale factor S is given in the top left corner of each panel and the scaled values for bulk density ρ_b and temperature T are indicated for each model fluid above the respective column. The results for the Yukawa liquid with inverse screening parameter $\kappa = 2/\sigma$ are qualitatively similar to those of the WCA liquid (second column Fig. 2 of the main text) but here with much longer-ranged decay behaviour. For identical dipolar strength $\mu/\sqrt{\epsilon\sigma^3} = 2$ the results for $g_{\nabla f \perp}(r)$ for both the soft-sphere dipolar fluid [58] and the Stockmayer fluid show strong signatures of chain formation, similar to the behaviour of the three-body gel former (fourth column of Fig. 2 of the main text). The Gay-Berne model (with parameters $\kappa = 3.8$, $\kappa' = 5$ [62]) features positive-valued $g_{\nabla f \perp}(r)$, which contrasts the behaviour of all other models and which we take to indicate interlocked arrangements of neighboring anisotropic molecules.

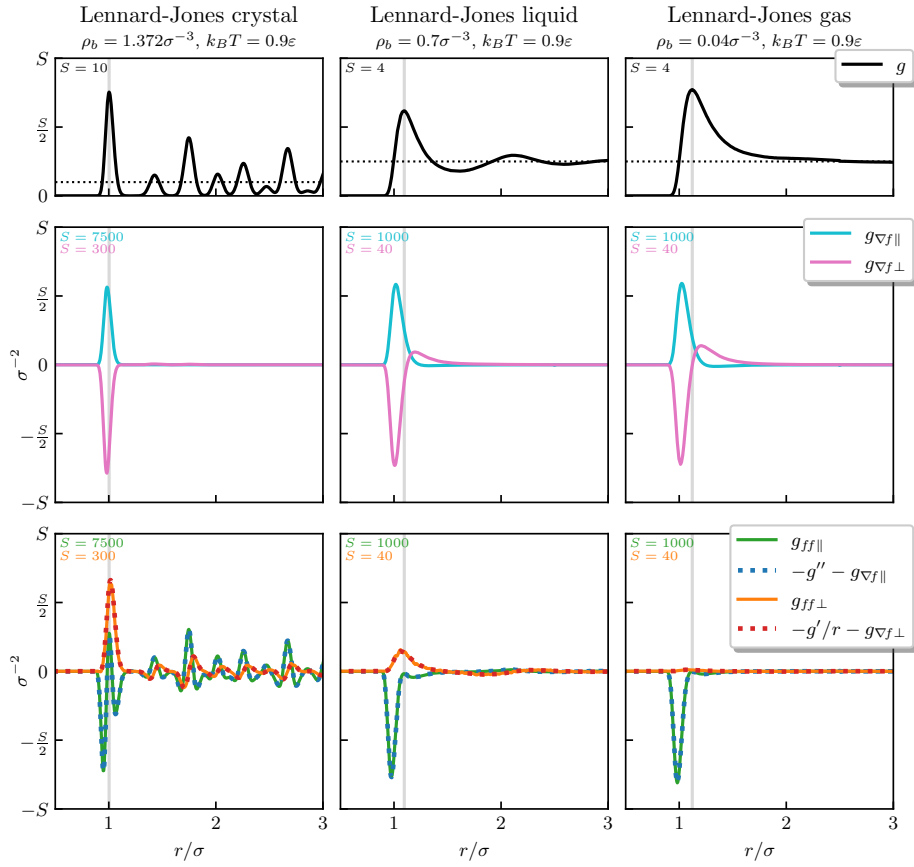


FIG. 4: Comparison of correlation functions for the LJ system in the fcc crystal phase (first column), the liquid (second column), and the gas phase (third column). Shown are the pair correlation function $g(r)$ (top row), the force-gradient correlator $\mathbf{g}_{\nabla f}(r)$ (middle row), and the force-force correlator $\mathbf{g}_{ff}(r)$ (bottom row). The plot style is analogous to Fig. 2 of the main text and to Fig. 3 of this SI. While the results for the gas and for the liquid carry the full structural two-body information, the correlators for the crystal are resolved only as a function of the radial distance r . This representation constitutes an average over global translations and rotations of the general inhomogeneous Noether sum rule, see Eq. (11) of the main text with $|\mathbf{r} - \mathbf{r}'|$ kept fixed. The reduced Noether identities (13) and (14) continue to hold in this averaged sense, as is demonstrated by the data collapse in the lower left panel. This perfect agreement serves as an indirect indication of the validity of the more general Eq. (11), which is applicable in the full inhomogeneous geometry.